

A nucleophilic beryllyl complex via metathesis at $[\text{Be}-\text{Be}]^{2+}$

Received: 12 January 2024

Accepted: 10 April 2024

Published online: 17 May 2024

Check for updates

Josef T. Boronski , Agamemnon E. Crumpton, Aisling F. Roper & Simon Aldridge

Owing to its high toxicity, the chemistry of element number four, beryllium, is poorly understood. However, as the lightest elements provide the basis for fundamental models of chemical bonding, there is a need for greater insight into the properties of beryllium. In this context, the chemistry of the homo-elemental Be–Be bond is of fundamental interest. Here the ligand metathesis chemistry of diberyllocene (**1**; Cp^*BeBeCp)—a stable complex with a Be–Be bond—has been investigated. These studies yield two complexes with Be–Be bonds: Cp^*BeBeCp (**2**) and $[\text{K}\{\text{HCDippN}\}_2\text{BO}\}_2]\text{BeBeCp}$ (**3**; Dipp = 2,6-diisopropylphenyl). Quantum chemical calculations indicate that the Be–Be bond in **3** is polarized to such an extent that the complex could be formulated as a mixed-oxidation state $\text{Be}^0/\text{Be}^{\text{II}}$ complex. Correspondingly, it is demonstrated that **3** can transfer the ‘beryllyl’ anion, $[\text{BeCp}]^-$, to an organic substrate, by analogy with the reactivity of sp^2 – sp^3 diboranes. Indeed, this work reveals striking similarities between the homo-elemental bonding linkages of beryllium and boron, despite the respective metallic and non-metallic natures of these elements.

The properties of the very lightest elements (that is, those with principal quantum numbers of 1 or 2) form the basis for fundamental models of chemical bonding and reactivity¹. It is notable, however, that the chemistry of the periodic table’s fourth element, beryllium, is very poorly developed owing to its extreme toxicity^{2–5}. One essential aspect of the element’s properties that long remained unexplored in the condensed phases was the chemistry of the homo-elemental Be–Be bond^{6–11}. In 1930, Herzberg unsuccessfully attempted to prepare diberyllium (Be_2) in the gas phase; this diatomic species (with a formal bond order of zero) was first spectroscopically identified in 2009^{12–14}. Moreover, despite numerous synthetic endeavours over the past 50 years, only in 2023 was the first example of a stable complex with a Be–Be bond—diberyllocene (Cp^*BeBeCp , **1**)—structurally characterized^{15–19}. Complex **1** is also a rare low-oxidation state beryllium species^{9,20}. Indeed, several recent studies have reported low-coordinate beryllium complexes bearing redox non-innocent carbene ligands^{21–26}. Although these have been formulated as ‘low valent’ beryllium complexes by some, such descriptions have been questioned by more recent theoretical studies^{20,27–30}.

In contrast to the recent discovery of **1**, stable complexes with Mg–Mg bonds were first reported in 2007^{31,32}. Attempts to prepare direct beryllium analogues of N-ligated magnesium(I) dimers were plagued by the formation of ligand- and solvent-activation products^{15–19}. Also of relevance are diborane(4) compounds, which feature B–B bonds and are isoelectronic with **1** (ref. 33). The first diborane(4) derivative, B_2Cl_4 , was prepared in 1925, and such species have subsequently found myriad applications in synthesis and catalysis. Quaternization of one of the boron centres of diborane(4) species by coordination of a nucleophile yields an sp^2 – sp^3 diborane, with a polarized (sp^2, δ^- ; sp^3, δ^+) B–B bond^{34,35}. As such, these species have been used for the metal-free delivery of the boryl $[\text{BR}_2]^-$ anion to organic substrates.

In this Article, we investigate the metathesis chemistry of the $[\text{Be}-\text{Be}]^{2+}$ core of **1** and report two complexes with Be–Be bonds: Cp^*BeBeCp (**2**) and $[\text{K}\{\text{HCDippN}\}_2\text{BO}\}_2]\text{BeBeCp}$ (**3**; Dipp = 2,6-diisopropylphenyl). These complexes are both unsymmetrical and, as a result, possess Be–Be bonds that are polarized, albeit to vastly differing degrees³⁴. In the case of **3**, quantum chemical calculations suggest that the uneven distribution of electron density could be rationalized

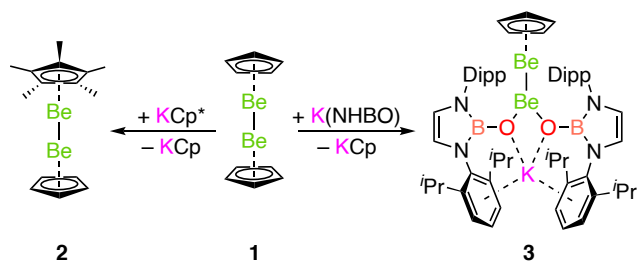


Fig. 1 | Synthesis of Cp^*BeBeCp (**2**) and $[\text{K}(\text{NHBO})_2]\text{BeBeCp}$ (**3**). Synthesis of complexes **2** and **3** via metathesis reactions with diberyllocene (**1**).

in terms of a mixed-valence $\text{Be}^0/\text{Be}^{\text{II}}$ formalism. This is supported by experimental studies, which reveal that **3** acts as a source of ‘beryllyl’ anions (formally featuring beryllium in the 0 oxidation state). Indeed, complex **3** is shown to transfer $[\text{BeCp}]^-$ to carbon electrophiles in a manner analogous to boryl anion, $[\text{BR}_2]^-$, transfer by sp^2 – sp^3 diboranes^{33,34,36}.

Results and discussion

Metathesis reactions of diberyllocene

Diberyllocene (**1**) and decamethylzincocene, $\text{Cp}^*\text{ZnZnCp}^*$ (**A**), are both calculated to feature robust homometallic bonds (homolytic bond dissociation energy for CpMMcP : $M = \text{Be}$, 71.7 kJ mol^{-1} ; $M = \text{Zn}$, 70.3 kJ mol^{-1})^{6,10,37}. Indeed, **A** has been found to participate in ligand metathesis reactions, which leave the Zn–Zn bond intact^{38–43}. Thus, we decided to investigate whether a salt metathesis approach would enable the substitution of the cyclopentadienyl ligands of **1** (refs. 18,44). Heating **1** and an excess of KCp^* in benzene for 4 days leads to the quantitative formation of Cp^*BeBeCp (**2**) and KCp (Fig. 1); no evidence for further substitution of the remaining Cp ligand was obtained even under forcing conditions. By contrast, reaction of **1** with two equivalents of the potassium salt of the N-heterocyclic boryloxy (NHBO) ligand $[\text{K}(\text{HCdippN})_2\text{BO}]$ is rapid, yielding $[\text{K}(\text{NHBO})_2]\text{BeBeCp}$ (**3**), again with the concomitant formation of KCp^* ⁴⁵ (Fig. 1). Both **2** and **3** could be crystallized from hexane and their molecular structures determined by single-crystal X-ray diffraction (SCXRD) (Figs. 2 and 3, respectively).

Complex **2**, like **1**, is a dimetalocene, consisting of two beryllium half-sandwich units—in this case one BeCp^* and one BeCp —linked by a Be–Be bond³⁷. There are two Cp^*BeBeCp molecules in the asymmetric unit of **2**. Of these two independent molecules, one exhibits a slightly staggered conformation of cyclopentadienyl ligands, whereas in the other complex, these carbocyclic ligands are almost perfectly eclipsed, as they are in **1**. The Be–Be distances measured for the two independent Cp^*BeBeCp units are $2.065(3) \text{ \AA}$ and $2.045(3) \text{ \AA}$, which are statistically indistinguishable from the Be–Be bond of **1** ($2.0545(18) \text{ \AA}$). Unlike in **1**, the orientations of the cyclopentadienyl ligands of the two molecules of **2** deviate somewhat from a parallel alignment, with interplanar angles of $8.71(9)^\circ$ and $12.84(10)^\circ$ (ref. 46). In addition, the Be– Cp_{cent} distances are $1.528(4) \text{ \AA}$ and $1.521(4) \text{ \AA}$, respectively, and the Be– $\text{Cp}^*_{\text{cent}}$ distances are $1.501(4) \text{ \AA}$ and $1.491(5) \text{ \AA}$, respectively. Hence, the Be– Cp_{cent} distances in **2** are comparable to the analogous metric measured for **1** ($1.519(3) \text{ \AA}$)¹⁸.

Complex **3** also features a BeCp unit, in addition to a $[\text{K}(\text{NHBO})_2]\text{Be}$ moiety, with two NHBO ligands coordinated to one Be centre through Be–O bonds⁴⁵. The two beryllium centres of **3** are connected to one another via a Be–Be bond. The two NHBO ligands of **3** also coordinate a potassium cation via $\text{K}\cdots(\eta^6\text{-C}_6\text{H}_3\text{iPr}_2)$ and $\text{K}\cdots\text{O}$ interactions, thereby forming a four-membered BeO_2K ring. The Be1–Be2 distance within **3** ($2.135(3) \text{ \AA}$) is markedly longer than those measured for **1** and **2** ($2.0545(18) \text{ \AA}$ and $2.045(3)/2.065(3) \text{ \AA}$, respectively)¹⁸. In addition, the Be– Cp_{cent} distance measured for **3** ($1.578(2) \text{ \AA}$) is considerably longer than the corresponding metrics for **1** and **2** ($1.519(3) \text{ \AA}$ and $1.528(4) \text{ \AA}$, respectively), suggesting that Be2 in **3** is highly electron rich. The Be1–O1 and $\text{K1}\cdots\text{O1}$ distances are $1.5639(14) \text{ \AA}$ and

$2.6561(8) \text{ \AA}$, respectively. This Be–O distance is somewhat longer than those reported for the three-coordinate beryllium(II) aryloxy complexes $\text{Be}(\text{ODipp})_2(\text{SIPr})$ ($1.497(3)/1.507(3) \text{ \AA}$; $\text{SIPr} = 1,3$ -diisopropyl-4,5-dimethylimidazol-2-ylidene) and $\text{Be}(\text{OMes}^*)_2(\text{Et}_2\text{O})$ ($1.481(2) \text{ \AA}$; $\text{Mes}^* = 2,4,6\text{-}^t\text{Bu}_3\text{C}_6\text{H}_2$), as well as for the homoleptic two-coordinate NHBO complex $\text{Be}(\text{NHBO})_2$ (**4**; $1.4266(8) \text{ \AA}$; vide infra), probably owing to the greater ionic radius of Be^{I} compared with Be^{II} (refs. 18,47,48). The O1–Be1–O1' angle in **3** is $107.88(7)^\circ$ and the sum of the angles at Be1 is $360.00(16)^\circ$, consistent with a trigonal planar geometry for this beryllium centre. This mirrors the trigonal planar geometry of the boron centres within diborane(4) derivatives³³.

It should be noted that ligand metathesis at a $[\text{Mg}^+\text{Mg}^{2+}]$ unit has not previously been reported³². Moreover, all structurally characterized magnesium(I) dimers feature supporting ligands with N-donor groups. Juxtaposing this, a variety of supporting ligands have been found to be suitable for stabilizing the Zn–Zn bond, including halides, aryloxides and even simple Lewis bases (for example, 4-dimethylaminopyridine and tetrahydrofuran)^{38–41,43}. The lability of **1** with respect to ligand metathesis (that is, the retention of the homometallic linkage) provides further experimental evidence for the theoretically predicted chemical similarities between the $[\text{Zn}^+\text{Zn}^{2+}]$ and $[\text{Be}^+\text{Be}^{2+}]$ moieties^{6,10}.

Complexes **2** and **3** were characterized by multinuclear NMR spectroscopy. Perhaps most informative are the ^9Be NMR chemical shifts measured for these complexes^{49,50}. The ^9Be NMR spectrum of complex **2** features resonances at -28.6 ppm and -21.7 ppm , attributable to the Cp-coordinated beryllium centre (Be_{Cp}) and Cp^* -coordinated beryllium centre (Be_{Cp^*}), respectively. These ^9Be NMR chemical shifts are very similar to those measured for the Be centres of **1** and BeCp^*_2 (-27.6 ppm and -21.7 ppm , respectively)^{18,51}. By contrast, in the case of **3**, disparate ^9Be NMR resonances are observed at -29.8 ppm and $+9.5 \text{ ppm}$, which correspond to Be_{Cp} and the NHBO-coordinated beryllium centre (Be_{NHBO}), respectively. The upfield resonance has the lowest chemical shift of any reported ^9Be NMR signal and indicates that Be_{Cp} is a highly electron-rich low-oxidation state beryllium centre^{18,44,49,50} (Supplementary Table 2 and Supplementary Fig. 20). The ^9Be NMR resonance corresponding to Be_{NHBO} is similar to that measured for the beryllium(II) complex $\text{Be}(\text{NHBO})_2$ (**4**, $+5.1 \text{ ppm}$; vide infra) and is extremely broad (full-width at half-maximum ($w_{1/2}$) 380 Hz), as is typically found for low-coordinate, electron-poor beryllium centres⁴⁹. For comparison, the $w_{1/2}$ of the ^9Be resonance measured for **1** is 33.4 Hz

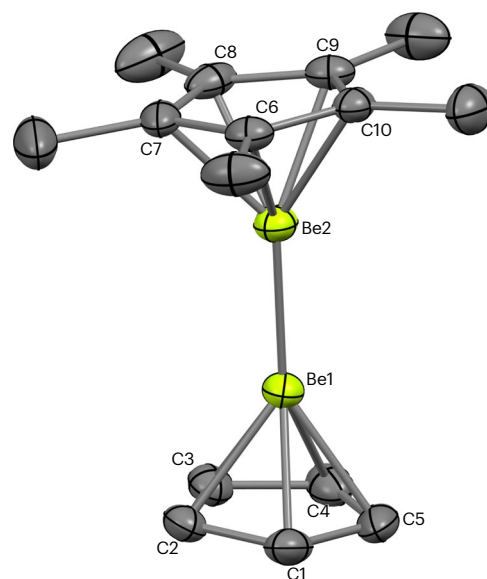


Fig. 2 | Molecular structure of complex **2**. Molecular structure of complex **2** in the solid state, as determined by X-ray crystallography. Thermal ellipsoids set at 50% probability and hydrogen atoms omitted for clarity.

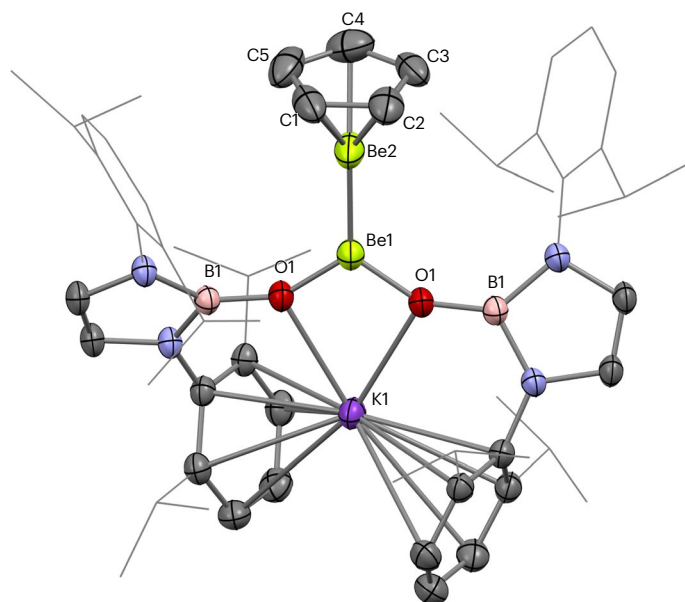


Fig. 3 | Molecular structure of 3. Molecular structure of complex **3** in the solid state, as determined by X-ray crystallography. Thermal ellipsoids set at 50% probability; selected substituents shown in wireframe format and hydrogen atoms omitted for clarity.

(ref. 18). No evidence of measurable Be–Be coupling could be observed in the ^9Be NMR spectra of either **2** or **3**.

Computational investigations of relevant complexes

To gain further insight into the electronic structure and bonding of **2** and **3**, both complexes were investigated using quantum chemical calculations. The structures of complexes **2** and **3** (and, for comparative purposes, **1**) were optimized with the $r^2\text{SCAN-3c}$ composite method, and a single-point calculation was performed on this optimized geometry using the $\omega\text{B97X-D4}$ functional with the def2-QZVPP basis set. The highest occupied molecular orbital (HOMO) of all three complexes corresponds to a Be–Be bonding orbital of σ -symmetry¹⁸. In the case of **1** and **2**, the HOMO is distributed equally between both beryllium centres (Supplementary Figs. 21 and 22). However, the HOMO of complex **3** has a hemispherical profile, with a greater proportion of the electron density localized on Be_{Cp} than on Be_{NHBO} , thus indicating that the Be–Be interaction in this complex is polarized¹ (Fig. 4).

To provide further evidence for this observation, quantum theory of atoms in molecules (QTAIM) and electron localization function (ELF) calculations were performed on **1**, **2** and **3**. In the case of **1** and **2**, QTAIM calculations find a (3, –3) critical point, or a non-nuclear attractor (NNA), in addition to two (3, –1) bond critical points, for the Be–Be interactions in both complexes (Supplementary Figs. 28 and 29). This is consistent with previous calculations on **1** and with experimental and theoretical studies of magnesium(I) dimers^{10,18,52}. By contrast, complex **3** is not calculated to feature an NNA, indicating fundamental differences between the Be–Be interaction in this complex and that in **1** and **2** (ref. 53) (Supplementary Fig. 30). The Bader charges calculated for the Be centres within **1** (+1.42) and **2** (Be_{Cp} , +1.39; Be_{Cp^*} , +1.43) are very similar, with the NNA bearing a large negative charge in both cases (**1**, –1.17; **2**, –1.15). Indeed, the Be–Be bond of **2** is clearly only very slightly polarized. In the case of **3**, however, the charge distribution at the beryllium centres is highly uneven (Be_{Cp} , +0.19; Be_{NHBO} , +1.62). The Bader charge for Be_{Cp} in **3** implies that this beryllium centre is extremely electron rich and is consistent with the upfield ^9Be NMR resonance and long $\text{Be}-\text{C}_{\text{cent}}$ distance measured for this complex^{54,55}. This charge distribution also aligns with the composition of the ELF basin associated with the Be–Be interaction in **3**, which features a much greater contribution from Be_{Cp}

($1.67 e^-$) than the Be_{NHBO} ($0.24 e^-$)^{56,57}. Combined, these data imply that complex **3** could be considered a mixed-valence $\text{Be}_{\text{Cp}}^0/\text{Be}_{\text{NHBO}}^{\text{II}}$ complex with a $\text{Be}^0 \rightarrow \text{Be}^{\text{II}}$ donor–acceptor bond^{56,57}.

Natural bond orbital (NBO) and natural population analysis (NPA) calculations also indicate that the Be–Be interaction in **3** is highly polarized; NPA charges of +0.64 for Be_{Cp} and +1.15 for Be_{NHBO} were calculated (Supplementary Figs. 33–35 and Supplementary Tables 6 and 7). In a similar fashion to the ELF calculations, NBO analysis indicates starkly different contributions to the Be–Be interaction from the two beryllium centres in **3**, with 62% of the electron density donated by Be_{Cp} and 38% by Be_{NHBO} ^{56,57}. The populations of the valence 2s and 2p orbitals of the two beryllium centres also evidence the greater degree of electron density at Be_{Cp} ($1.34 e^-$) compared with Be_{NHBO} ($0.85 e^-$).

To obtain further evidence for the polarized nature of the Be–Be interaction in **3**, the SCXRD-derived residual electron density map for this complex (refined using non-spherical atomic form factors) was examined^{52,58,59}. There is a resemblance between the residual electron density in this plot and the profile of the ELF isosurface corresponding to the Be–Be bonding basin (Fig. 5). Indeed, in both cases, the electron density appears to be polarized, with a hemispherical lobe directed from Be_{Cp} towards Be_{NHBO} . To benchmark the ELF data for **3**, the isosurfaces corresponding to the B–B bond of sp^2-sp^3 diborane [(pin)B–B(F)(pin)][–] (**B**; pin = $[\{\text{OC}(\text{Me})_2\}_2]^{2-}$) and the archetypal donor–acceptor N–B bond of H_3NBH_3 (**C**) were plotted using the same method³⁵ (Supplementary Figs. 36 and 37). Visually, these two ELF isosurfaces, and that of the Be–Be interaction in **3**, have similar hemispherical profiles, with the electron density directed from the Lewis basic moiety towards the Lewis acidic centre. This topology is typical of the forms of ELF isosurfaces for donor–acceptor interactions^{56–58}. It should be noted that the ELF isosurfaces for the Be–Be interaction **1** and **2** (as well as a range of polarized and non-polarized C–C bonds) have symmetrical, pancake-like profiles, which are typical of covalent-type bonds and are therefore markedly different from that of **3** (ref. 58) (Supplementary Figs. 31, 32 and 38–40).

To further examine the nature of the Be–Be interaction in **3** computationally, energy decomposition analysis (EDA) calculations were performed on this complex, as well as **1**, **2**, **B** and **C**. It has previously been found (by ourselves and others) that natural energy

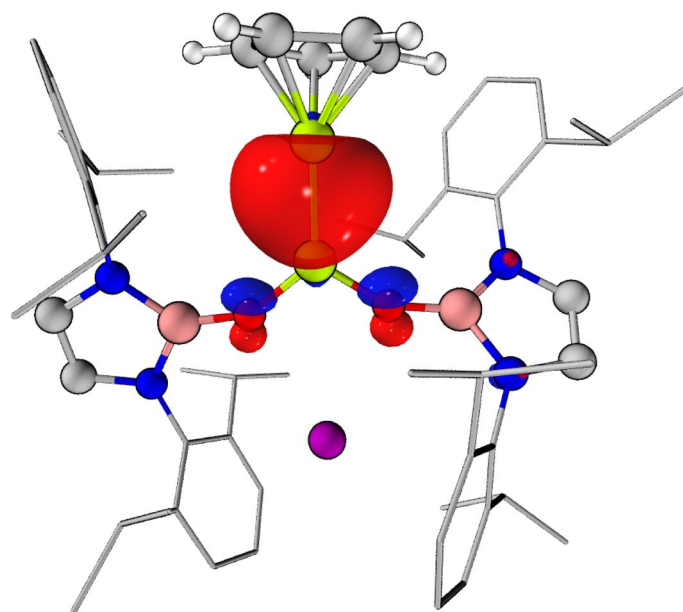


Fig. 4 | HOMO of compound 3. HOMO of complex **3**, corresponding to the principal Be–Be bonding interaction (0.05 a.u.). Complex geometry optimized with the $r^2\text{SCAN-3c}$ composite method, followed by a single-point calculation using the $\omega\text{B97X-D4}$ functional with the def2-QZVPP basis set.

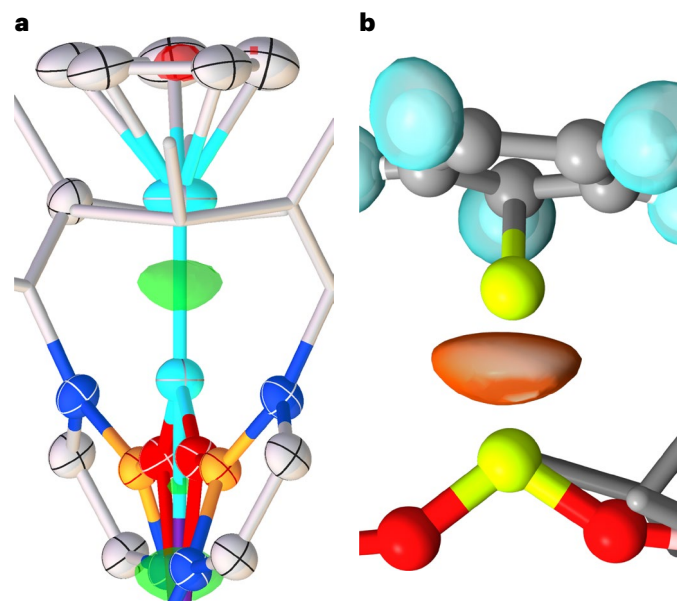


Fig. 5 | Experimental and computational analysis of Be–Be bonding in complex 3. **a**, The SCXRD-derived residual electron density plot for complex 3. **b**, ELF isosurface for the Be–Be interaction in 3 (right; orange; 0.7 a.u.).

decomposition analysis (NEDA) is effective for probing the nature of bonding in main group element-containing molecules; thus, we used this technique here^{60,61} (Supplementary Tables 8–12). The most representative bonding model for a given molecule can be determined by the fragments that yield the lowest magnitude of the orbital interaction energy (E_{orb}) upon recombination^{20,27,28,62–64}. Indeed, in the case of **3**, $|E_{orb}|$ for a donor–acceptor recombination ($[\text{CpBe}] \rightarrow [\text{Be}(\text{NHBO})_2\text{K}]$, $-217 \text{ kcal mol}^{-1}$) is lower than that of the (homolytic) radical recombination of the Be–Be linkage ($-282 \text{ kcal mol}^{-1}$). This mirrors calculations performed on **B** and **C**, for which $|E_{orb}|$ for the donor–acceptor recombination ($[(\text{pin})\text{B} \rightarrow \text{B}(\text{F})(\text{pin})]^-$, $-411 \text{ kcal mol}^{-1}$; $\text{H}_3\text{N} \rightarrow \text{BH}_3$, $-216 \text{ kcal mol}^{-1}$) is lower, in each case, than the respective homolytic radical recombinations ($-521 \text{ kcal mol}^{-1}$ and $-532 \text{ kcal mol}^{-1}$, respectively). This contrasts with the corresponding analysis on **2**, for which a homolytic radical Be–Be recombination is favoured ($E_{orb} = -224 \text{ kcal mol}^{-1}$), compared with both donor–acceptor formulations for the complex ($[\text{CpBe}] \rightarrow [\text{BeCp}^*]$, $-275 \text{ kcal mol}^{-1}$; $[\text{Cp}^*\text{Be}] \rightarrow [\text{BeCp}]$, $-276 \text{ kcal mol}^{-1}$). Hence, NEDA also indicates that a donor–acceptor, $\text{Be}^0/\text{Be}^{\text{II}}$ formalism could be used to describe the electronic configuration of **3** (ref. 27).

EDA coupled with natural orbitals for chemical valence (EDA–NOCV) calculations were also performed on **1**, **2** and **3** (ref. 1). The $|E_{orb}|$ for the (homolytic) biradical fragmentation of the Be–Be linkage of **3** ($-70.1 \text{ kcal mol}^{-1}$; Supplementary Figs. 47 and 48) is lower than the corresponding $|E_{orb}|$ for a pure donor–acceptor fragmentation ($[\text{CpBe}] \rightarrow [\text{Be}(\text{NHBO})_2\text{K}]$, $-116 \text{ kcal mol}^{-1}$; Supplementary Fig. 49). Nonetheless, in the case of homolytic fragmentation, the eigenvalues for the α_1 - and β_1 -pair densities are highly dissimilar ($[\text{CpBe}] \rightarrow [\text{Be}(\text{NHBO})_2\text{K}]$, 0.36; $[\text{CpBe}] \leftarrow [\text{Be}(\text{NHBO})_2\text{K}]$, 0.29), thereby indicating that there is a large net movement of electrons from Be_{Cp} to Be_{NHBO} (Supplementary Table 15). Again, this evidences the highly polarized nature of the Be–Be linkage in **3**. For reference, EDA–NOCV calculations were also performed on a range of other molecules with polar and non-polar homo-elemental (B–B and C–C) bonds (Supplementary Tables 14–16 and Supplementary Figs. 50–61). Of all these examples, homolytic fragmentation of the Be–Be bond of **3** was calculated to lead to the greatest net movement of electrons. Thus, the Be–Be linkage of **3** could be described as the most polarized bond of all those studied here.

When complexes of the form $[\text{Be}(\text{cAAC})_2]$ (**D**; cAAC = cyclic(alkyl)(amino)carbene) were initially reported, they were described as comprising a neutral beryllium(0) centre and two neutral carbene ligands²¹. However, cAAC ligands are known to be redox non-innocent, and several subsequent theoretical studies indicate that **D** is instead best described as a beryllium(II) complex featuring two anionic cAAC ligands^{20,29}. Indeed, this is consistent with our own calculations on **D**, which yield Bader and NPA charges of +1.50 and +1.47, respectively, for the beryllium centre within this complex. These values are much greater than the same metrics calculated for Be_{Cp} in **3** (+0.19 and +0.64, respectively). In broader terms, the formal oxidation state assignment for a particular element centre is only meaningful in the context of its chemical behaviour. Indeed, although **D** has been used as a reducing agent, this reactivity could be ascribed to the anionic nature of the carbene ligands within this complex²⁵. As far as we are aware, there are no reported data that unequivocally show that **D** reacts as a source of low-valent beryllium.

Reactivity studies of complex 3

To obtain experimental evidence for the possible $\text{Be}^0/\text{Be}^{\text{II}}$ formulation for **3**, the reactivity of this complex was examined. In this context, the reaction of **3** with $[\text{CPh}_3][\text{B}(\text{C}_6\text{F}_5)_4]$ is informative: the process leads to the formation of previously unreported complexes $\text{Be}(\text{NHBO})_2$ (**4**; Supplementary Fig. 15) and $\text{CpBe}(\text{CPh}_3)$ (**5**; Supplementary Fig. 16), as well as $\text{K}[\text{B}(\text{C}_6\text{F}_5)_4]$ (Fig. 6). This reaction involves the transfer of a nucleophilic ‘beryllyl’ anion, $[\text{CpBe}]^-$ (which features a formal beryllium(0) centre), from **3** to the electrophilic trityl cation, forming a Be–C bond and yielding **5**, leaving the beryllium(II)-containing fragment **4** (ref. 44). This reactivity is analogous to that of sp^2 – sp^3 diboranes, which feature highly polarized B–B bonds and act as a source of the boryl anion, $[\text{BR}_2]^-$, which is closely related to the beryllyl anion^{33–36}. As such, the observed reactivity of **3** provides evidence that this species could be considered a mixed-oxidation state $\text{Be}^0/\text{Be}^{\text{II}}$ complex, and is a rare example of a nucleophilic s-block complex.

Conclusion

We have prepared two complexes with Be–Be bonds through ligand metathesis reactions of diberyllocene (CpBeBeCp , **1**). These complexes— Cp^*BeBeCp (**2**) and $[\text{K}\{\text{HCDippN}\}_2\text{BO}\}_2]\text{BeBeCp}$ (**3**)—have been studied by quantum chemical methods, which imply that **3** could be formulated as a $\text{Be}^0/\text{Be}^{\text{II}}$ complex. This assignment is supported by quantum chemical calculations and residual electron density plots, which are derived from SCXRD measurements. Further experimental evidence for this claim has been obtained through transfer of the beryllyl anion, $[\text{CpBe}]^-$, to an electrophilic organic substrate and isolation of both beryllium-containing products. Fundamentally, this reactivity can be likened to that of sp^2 – sp^3 diboranes, revealing that the reactivities of homo-elemental bonds of beryllium and boron have parallels, despite the respective metallic and non-metallic natures of these elements. Hence, this work reveals that bonding trends across period 2 are more continuous than may previously have been appreciated. We continue to investigate the chemical relationships between beryllium and its neighbouring elements to test models of chemical bonding.

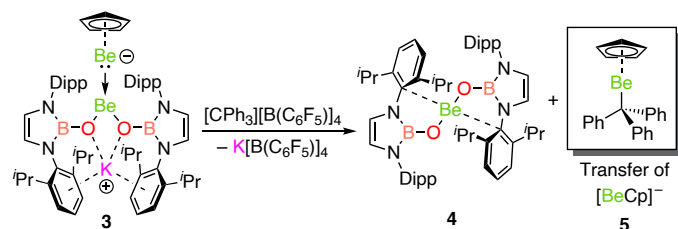


Fig. 6 | Transfer of the beryllyl anion, $[\text{CpBe}]^-$, to an organic substrate by complex 3. Reactivity of complex **3** with $[\text{CPh}_3][\text{B}(\text{C}_6\text{F}_5)_4]$, a source of the organic electrophile $[\text{CPh}_3]^+$.

Online content

Any methods, additional references, Nature Portfolio reporting summaries, source data, extended data, supplementary information, acknowledgements, peer review information; details of author contributions and competing interests; and statements of data and code availability are available at <https://doi.org/10.1038/s41557-024-01534-9>.

References

- Zhao, L., Pan, S., Holzmann, N., Schwerdtfeger, P. & Frenking, G. Chemical bonding and bonding models of main-group compounds. *Chem. Rev.* **119**, 8781–8845 (2019).
- Buchner, M. R. Recent contributions to the coordination chemistry of beryllium. *Chem. Eur. J.* **25**, 12018–12036 (2019).
- Buchner, M. R. Beryllium coordination chemistry and its implications on the understanding of metal induced immune responses. *Chem. Commun.* **56**, 8895–8907 (2020).
- Naglav, D., Buchner, M. R., Bendt, G., Kraus, F. & Schulz, S. Off the beaten track—a hitchhiker’s guide to beryllium chemistry. *Angew. Chem. Int. Ed.* **55**, 10562–10576 (2016).
- Buchner, M. R. & Müller, M. Handling beryllium, the safe way. *ACS Chem. Health Saf.* **30**, 36–43 (2023).
- Velazquez, A., Fernández, I., Frenking, G. & Merino, G. Multimetalloenes. A theoretical study. *Organometallics* **26**, 4731–4736 (2007).
- Xie, Y., Schaefer, H. F. & Jemmis, E. D. Characteristics of novel sandwiched beryllium, magnesium, and calcium dimers: $C_5H_5BeBeC_5H_5$, $C_5H_5MgMgC_5H_5$, and $C_5H_5CaCaC_5H_5$. *Chem. Phys. Lett.* **402**, 414–421 (2005).
- Kalemos, A. The nature of the chemical bond in Be_2^+ , Be_2 , Be_2^- , and Be_3 . *J. Chem. Phys.* **145**, 214302 (2016).
- Couchman, S. A., Holzmann, N., Frenking, G., Wilson, D. J. D. & Dutton, J. L. Beryllium chemistry the safe way: a theoretical evaluation of low oxidation state beryllium compounds. *Dalton Trans.* **42**, 11375–11384 (2013).
- Gosch, M. A. & Wilson, D. J. D. Heteronuclear and homonuclear bimetallic metalloenes of alkaline earths and zinc. *Organometallics* **42**, 2185–2196 (2023).
- Tague, T. J. & Andrews, L. Reactions of beryllium atoms with hydrogen. Matrix infrared spectra of novel product molecules. *J. Am. Chem. Soc.* **115**, 12111–12116 (1993).
- Herzberg, G. Zum Aufbau der zweiatomigen Moleküle. *Z. Phys.* **57**, 601–630 (1929).
- Merritt, J. M., Bondybey, V. E. & Heaven, M. C. Beryllium dimer—caught in the act of bonding. *Science* **324**, 1548–1551 (2009).
- Patkowski, K., Špirko, V. & Szalewicz, K. On the elusive twelfth vibrational state of beryllium dimer. *Science* **326**, 1382–1384 (2009).
- Bonyhady, S. J. et al. β -Diketiminato-stabilized magnesium(I) dimers and magnesium(II) hydride complexes: synthesis, characterization, adduct formation, and reactivity studies. *Chem. Eur. J.* **16**, 938–955 (2010).
- Pearce, K. G., Hill, M. S. & Mahon, M. F. Beryllium-centred C–H activation of benzene. *Chem. Commun.* **59**, 1453–1456 (2023).
- Arrowsmith, M. et al. Three-coordinate beryllium β -diketiminates: synthesis and reduction chemistry. *Inorg. Chem.* **51**, 13408–13418 (2012).
- Boronski, J. T., Crumpton, A. E., Wales, L. L. & Aldridge, S. Diberyllocene, a stable compound of Be(I) with a Be–Be bond. *Science* **380**, 1147–1149 (2023).
- Boronski, J. T. Alkaline earth metals: homometallic bonding. *Dalton Trans.* **53**, 33–39 (2024).
- Gimferrer, M. et al. The oxidation state in low-valent beryllium and magnesium compounds. *Chem. Sci.* **13**, 6583–6591 (2022).
- Arrowsmith, M. et al. Neutral zero-valent s-block complexes with strong multiple bonding. *Nat. Chem.* **8**, 890–894 (2016).
- Czernetzki, C. et al. A neutral beryllium(I) radical. *Angew. Chem. Int. Ed.* **60**, 20776–20780 (2021).
- Czernetzki, C., Arrowsmith, M., Endres, L., Kruppenacher, I. & Braunschweig, H. Tricoordinate beryllium radicals and their reactivity. *Inorg. Chem.* **63**, 2670–2678 (2024).
- Wang, G. et al. A stable, crystalline beryllium radical cation. *J. Am. Chem. Soc.* **142**, 4560–4564 (2020).
- Freeman, L. A., Walley, J. E. & Gilliard, R. J. Synthesis and reactivity of low-oxidation-state alkaline earth metal complexes. *Nat. Synth.* **1**, 439–448 (2022).
- Parveen, D., Yadav, R. K. & Roy, D. K. Recent progress in beryllium organometallic chemistry. *Chem. Commun.* **60**, 1663–1673 (2024).
- Pan, S. & Frenking, G. Comment on “The oxidation state in low-valent beryllium and magnesium compounds” by M. Gimferrer, S. Danés, E. Vos, C. B. Yildiz, I. Corral, A. Jana, P. Salvador and D. M. Andrada. *Chem. Sci.* **2022**, 13, 6583. *Chem. Sci.* **14**, 379–383 (2023).
- Gimferrer, M. et al. Reply to the ‘Comment on “The oxidation state in low-valent beryllium and magnesium compounds”’ by S. Pan and G. Frenking. *Chem. Sci.* **2022**, 13, DOI: 10.1039/D2SC04231B. *Chem. Sci.* **14**, 384–392 (2023).
- Jędrzkiewicz, D. et al. Access to a labile monomeric magnesium radical by ball-milling. *Angew. Chem. Int. Ed.* **61**, e202200511 (2022).
- Parkin, G. Impact of the coordination of multiple Lewis acid functions on the electronic structure and v^f configuration of a metal center. *Dalton Trans.* **51**, 411–427 (2022).
- Green, S. P., Jones, C. & Stasch, A. Stable magnesium(I) compounds with Mg–Mg bonds. *Science* **318**, 1754–1757 (2007).
- Jones, C. Dimeric magnesium(I) β -diketiminates: a new class of quasi-universal reducing agent. *Nat. Rev. Chem.* **1**, 0059 (2017).
- Neeve, E. C., Geier, S. J., Mkhali, I. A. I., Westcott, S. A. & Marder, T. B. Diboron(4) compounds: from structural curiosity to synthetic workhorse. *Chem. Rev.* **116**, 9091–9161 (2016).
- Dewhurst, R. D., Neeve, E. C., Braunschweig, H. & Marder, T. B. sp^2 – sp^3 diboranes: astounding structural variability and mild sources of nucleophilic boron for organic synthesis. *Chem. Commun.* **51**, 9594–9607 (2015).
- Pietsch, S. et al. Synthesis, structure, and reactivity of anionic sp^2 – sp^3 diboron compounds: readily accessible boryl nucleophiles. *Chem. Eur. J.* **21**, 7082–7098 (2015).
- Pécharman, A.-F. et al. Easy access to nucleophilic boron through diborane to magnesium boryl metathesis. *Nat. Commun.* **8**, 15022 (2017).
- Resa, I., Carmona, E., Gutierrez-Puebla, E. & Monge, A. Decamethylidzincocene, a stable compound of Zn(I) with a Zn–Zn bond. *Science* **305**, 1136–1138 (2004).
- Hicks, J., Underhill, E. J., Kefalidis, C. E., Maron, L. & Jones, C. A mixed-valence tri-zinc complex, $[LZnZnZnL]$ (L = bulky amide), bearing a linear chain of two-coordinate zinc atoms. *Angew. Chem. Int. Ed.* **54**, 10000–10004 (2015).
- Schulz, S. et al. Structural characterization of a base-stabilized $[Zn_2]^{2+}$ cation. *Angew. Chem. Int. Ed.* **48**, 5748–5751 (2009).
- Freitag, K. et al. Cp* as a removable protecting group: low valent Zn(I) compounds by reductive elimination, protolytic and oxidative cleavage of Zn–Cp*. *Dalton Trans.* **42**, 10540 (2013).
- Banh, H., Gemel, C., Seidel, R. W. & Fischer, R. A. A solvated zinc analogue of the calomel-dication. *Chem. Commun.* **51**, 2170–2172 (2015).
- Schulz, S., Schuchmann, D., Westphal, U. & Bolte, M. Dizincocene as a building block for novel Zn–Zn-bonded compounds? *Organometallics* **28**, 1590–1592 (2009).
- Carrasco, M. et al. Zn–Zn-bonded compounds that contain monoanionic oxygen-donor ligands. *Chem. Eur. J.* **16**, 9754–9757 (2010).

44. Boronski, J. T. et al. Inducing nucleophilic reactivity at beryllium with an aluminyl ligand. *J. Am. Chem. Soc.* **145**, 4408–4413 (2023).
45. Loh, Y. K., Ying, L., Ángeles Fuentes, M., Do, D. C. H. & Aldridge, S. An N-heterocyclic boryloxy ligand isoelectronic with N-heterocyclic imines: access to an acyclic dioxysilylene and its heavier congeners. *Angew. Chem. Int. Ed.* **58**, 4847–4851 (2019).
46. Grirrane, A. et al. Zinc–zinc bonded zincocene structures. Synthesis and characterization of $Zn_2(\eta^5-C_5Me_5)_2$ and $Zn_2(\eta^5-C_5Me_4Et)_2$. *J. Am. Chem. Soc.* **129**, 693–703 (2007).
47. Walley, J. E., Wong, Y., Freeman, L. A., Dickie, D. A. & Gilliard, R. J. N-Heterocyclic carbene-supported aryl- and alk- oxides of beryllium and magnesium. *Catalysts* **9**, 934 (2019).
48. Ruhlandt-Senge, K., Bartlett, R. A., Olmstead, M. M. & Power, P. P. Synthesis and structural characterization of the beryllium compounds $[Be(2,4,6-Me_3C_6H_2)_2(OEt)_2]$, $[Be\{O(2,4,6-tert-Bu_3C_6H_2)\}_2(OEt)_2]$, and $[Be\{S(2,4,6-tert-Bu_3C_6H_2)\}_2(THF)]$.cndot.PhMe and determination of the structure of $[BeCl_2(OEt)_2]$. *Inorg. Chem.* **32**, 1724–1728 (1993).
49. Buchanan, J. K. & Plieger, P. G. 9Be nuclear magnetic resonance spectroscopy trends in discrete complexes: an update. *Z. Naturforsch. B* **75**, 459–472 (2020).
50. Plieger, P. G. et al. Predicting 9Be nuclear magnetic resonance chemical shielding tensors utilizing density functional theory. *J. Am. Chem. Soc.* **126**, 14651–14658 (2004).
51. del Mar Conejo, M. et al. Synthesis, solid-state structure, and bonding analysis of the beryllocenes $[Be(C_5Me_4H)_2]$, $[Be(C_5Me_5)_2]$, and $[Be(C_5Me_5)(C_5Me_4H)]$. *Chem. Eur. J.* **9**, 4452–4461 (2003).
52. Platts, J. A., Overgaard, J., Jones, C., Iversen, B. B. & Stasch, A. First experimental characterization of a non-nuclear attractor in a dimeric magnesium(I) compound. *J. Phys. Chem. A* **115**, 194–200 (2011).
53. Liu, H.-Y. et al. Reductive dimerization of CO by a Na/Mg(I) diamide. *J. Am. Chem. Soc.* **143**, 17851–17856 (2021).
54. Timoshkin, A. Y. & Schaefer, H. F. Donor–acceptor sandwiches of main-group elements. *Organometallics* **24**, 3343–3345 (2005).
55. Jansen, G. et al. Unsupported Ti–Co and Zr–Co bonds in heterobimetallic complexes: a theoretical description of metal–metal bond polarity. *J. Am. Chem. Soc.* **120**, 7239–7251 (1998).
56. Dang, Y., Meng, L., Qin, M., Li, Q. & Li, X. Stability and donor–acceptor bond in dinuclear organometallics $CpM_1-M_2Cl_3$ ($M_1, M_2 = B, Al, Ga, In; Cp = \eta^5-C_5H_5$). *J. Mol. Model.* **24**, 7 (2018).
57. Huo, S., Meng, D., Zhang, X., Meng, L. & Li, X. Bonding analysis of the donor–acceptor sandwiches $CpE-MCp$ ($E = B, Al, Ga; M = Li, Na, K; Cp = \eta^5-C_5H_5$). *J. Mol. Model.* **20**, 2455 (2014).
58. Bianchi, R., Gervasio, G. & Marabello, D. Experimental electron density analysis of $Mn_2(CO)_{10}$: metal–metal and metal–ligand bond characterization. *Inorg. Chem.* **39**, 2360–2366 (2000).
59. Kleemiss, F. et al. Accurate crystal structures and chemical properties from NoSpherA2. *Chem. Sci.* **12**, 1675–1692 (2021).
60. Zheng, X., Crumpton, A. E., Ellwanger, M. A. & Aldridge, S. A planar per-borylated digermene. *Dalton Trans.* **52**, 16591–16595 (2023).
61. Li, T.-L. & Lu, W.-C. Energy decomposition analysis of cationic carbene analogues with group 13 and 16 elements as a central atom: a comparative study. *Phys. Chem. Chem. Phys.* **24**, 8970–8978 (2022).
62. Hermann, M. & Frenking, G. Carbones as ligands in novel main-group compounds $E[C(NHC)_2]_2$ ($E = Be, B^+, C^{2+}, N^{3+}, Mg, Al^+, Si^{2+}, P^{3+}$): a theoretical study. *Chem. Eur. J.* **23**, 3347–3356 (2017).
63. Zhang, Q. et al. Formation and characterization of the boron dicarbonyl complex $[B(CO)_2]^-$. *Angew. Chem. Int. Ed.* **54**, 11078–11083 (2015).
64. Scharf, L. T., Andrada, D. M., Frenking, G. & Gessner, V. H. The bonding situation in metalated ylides. *Chem. Eur. J.* **23**, 4422–4434 (2017).

Publisher's note Springer Nature remains neutral with regard to jurisdictional claims in published maps and institutional affiliations.

Open Access This article is licensed under a Creative Commons Attribution 4.0 International License, which permits use, sharing, adaptation, distribution and reproduction in any medium or format, as long as you give appropriate credit to the original author(s) and the source, provide a link to the Creative Commons licence, and indicate if changes were made. The images or other third party material in this article are included in the article's Creative Commons licence, unless indicated otherwise in a credit line to the material. If material is not included in the article's Creative Commons licence and your intended use is not permitted by statutory regulation or exceeds the permitted use, you will need to obtain permission directly from the copyright holder. To view a copy of this licence, visit <http://creativecommons.org/licenses/by/4.0/>.

© The Author(s) 2024

Methods

General considerations

Beryllium and its compounds are extremely toxic and can cause irreversible health effects through inhalation or skin contact. The work with beryllium-containing materials described herein was carried out by trained operators, with strict adherence to local and national rules and regulations⁵.

All manipulations were carried out using Schlenk line or glovebox techniques under an atmosphere of argon or dinitrogen. Solvents were dried by passage through activated alumina towers, dried with NaK₂ and degassed before use. Solvents were stored over NaK₂. NMR spectra were measured in C₆D₆, which was dried over NaK₂, with the solvent being distilled under reduced pressure, degassed by three freeze–pump–thaw cycles and stored under argon in a Teflon valve ampoule. NMR samples were prepared under argon in 5 mm Wilmad 507-PP tubes fitted with J. Young Teflon valves. NMR spectra were measured on a Bruker Avance III HD Nanobay 400 MHz NMR spectrometer equipped with a 9.4 T magnet or a Bruker Avance III 500 MHz NMR spectrometer equipped with an 11.75 T magnet. ¹H and ¹³C NMR spectra were referenced internally to residual protio-solvent (¹H) or solvent (¹³C) resonances and are reported relative to tetramethylsilane ($\delta = 0$ ppm). ⁹Be NMR spectra were referenced to a 0.43 M solution of BeSO₄·4H₂O in D₂O ($\delta = 0$ ppm). Chemical shifts are quoted in δ (ppm) and coupling constants in Hz. The compounds diberyllocene (**1**), [(HCDippN)₂BO]₂K (K-NHBO), KCp* and [CPh₃][B(C₆F₅)₄] were prepared as described previously^{18,45,65}.

Synthesis of novel compounds

Synthesis of Cp*BeBeCp (2). A solid mixture of **1** (4.0 mg, 0.027 mmol) and KCp* (19 mg, 0.11 mmol, 4.0 equiv.) was added to an ampoule fitted with a Teflon valve and equipped with a glass-coated stirrer bar. Benzene (1 ml) was condensed into the vessel in vacuo at –196 °C. The colourless suspension was allowed to warm to room temperature and stirred at 80 °C for 4 days. Volatiles were removed in vacuo at 0 °C, leaving a white powder. Complex **2** is volatile, so prolonged drying should be avoided. Soluble material was dissolved in hexane (0.5 ml), filtered and concentrated (0.2 ml). Concentration of a hexane solution in a sealed glass λ -type tube resulted in the formation of colourless crystals, which were carefully dried in vacuo. Yield: 4.0 mg, 68%. Single crystals of **2** suitable for X-ray diffraction experiments were obtained by slow concentration of a hexane solution in a sealed glass λ -type tube. Analytically calculated for C₁₅H₂₀Be₂: C, 82.51; H, 9.23. Found: C, 81.96; H, 9.16. ¹H NMR (400 MHz, C₆D₆, 298 K): $\delta = 1.90$ (s, 15H, C₅(CH₃)₅), 5.68 (s, 5H, C₅H₅); ⁹Be NMR (42 MHz, C₆D₆): $\delta = -28.6$ ($w_{1/2} = 49.3$ Hz; CpBe), -21.7 ($w_{1/2} = 39.9$ Hz; Cp*Be); ¹³C{¹H} NMR (101 MHz, C₆D₆): $\delta = 10.3$ (C₅(CH₃)₅), 102.3 (C₅H₅), 108.2 (C₅(CH₃)₅).

Synthesis of [K{(HCDippN)₂BO}]₂BeBeCp (3). A solid mixture of **1** (4.0 mg, 0.027 mmol) and K-NHBO (23 mg, 0.054 mmol, 2.0 equiv.) was added to an ampoule fitted with a Teflon valve and equipped with a glass-coated stirrer bar. Benzene (1 ml) was condensed into the vessel in vacuo at –196 °C. The pale-yellow suspension was allowed to warm to room temperature and stirred for 1 h. Subsequently, volatiles were removed in vacuo, and soluble material was dissolved in hexane (0.5 ml). The suspension was filtered and concentrated (0.2 ml). Concentration of a hexane solution in a sealed glass λ -type tube resulted in the formation of colourless crystals, which were carefully dried in vacuo. Yield: 18 mg, 73%. Single crystals of **3** suitable for X-ray diffraction experiments were obtained by slow concentration of a hexane solution in a sealed glass λ -type tube. Analytically calculated for C₅₇H₇₇B₂Be₂KN₄O₂: C, 73.69; H, 8.35; N, 6.03. Found: C, 73.32; H, 8.11; N, 5.85. ¹H NMR (400 MHz, C₆D₆, 298 K): $\delta = 1.20$ (2x d, 48H, CH(CH₃)₂), 3.49 (sept, ³J_{HH} = 6.8 Hz, 8H, CH(CH₃)₂), 5.49 (s, 5H, C₅H₅), 5.93 (s, 4H, CH), 7.06 (m, 12H, ArH); ⁹Be NMR (42 MHz, C₆D₆): $\delta = -29.8$ ($w_{1/2} = 94.7$ Hz; CpBe), 9.5 ($w_{1/2} = 380$ Hz; O₂Be); ¹¹B NMR (128 MHz, C₆D₆): $\delta = 20.5$; ¹³C{¹H} NMR (101 MHz, C₆D₆): $\delta = 23.7$ (CH(CH₃)₂), 24.6 (CH(CH₃)₂), 28.3 (CH(CH₃)₂),

102.7 (C₅H₅), 116.5 (NCH), 123.7 (Dipp-*m*-CH), 126.4 (Dipp-*p*-CH), 141.9 (Dipp-*i*-C), 147.4 (Dipp-*o*-C).

Synthesis of Be(NHBO)₂ (4) and CpBe(CPh₃) (5). A solid mixture of **3** (8.0 mg, 0.0086 mmol) and [CPh₃][B(C₆F₅)₄] (7.9 mg, 0.0086 mmol) was added to an ampoule fitted with a Teflon valve and equipped with a glass-coated stirrer bar. Benzene (1 ml) was condensed into the vessel in vacuo at –196 °C. The yellow solution was allowed to warm to room temperature and stirred for 1 h. Subsequently, volatiles were removed in vacuo, soluble material was dissolved in hexane (0.5 ml), and the suspension was filtered. Slow concentration of the resulting solution in a sealed glass λ -type tube led to the formation of colourless crystals (**4**) and yellow crystals (**5**), which were manually separated. Compounds **4** and **5** degrade rapidly in the solid state and in solution. Yield of **4**: 3.8 mg, 54%. Yield of **5**: 2.1 mg, 76%. Compound **4**: analytically calculated for C₅₂H₇₂B₂BeN₄O₂: C, 76.56; H, 8.90; N, 6.87. Found: C, 76.39; H, 8.86; N, 6.74. ¹H NMR (400 MHz, C₆D₆, 298 K): $\delta = 1.04$ (d, ³J_{HH} = 7.1 Hz, 24H, CH(CH₃)₂), 1.19 (d, ³J_{HH} = 6.8 Hz, 24H, CH(CH₃)₂), 3.16 (sept, ³J_{HH} = 7.5 Hz, 8H, CH(CH₃)₂), 5.86 (s, 4H, CH), 7.09 (m, 12H, ArH); ⁹Be NMR (42 MHz, C₆D₆): $\delta = 5.1$ ($w_{1/2} = 727.4$ Hz); ¹¹B NMR (128 MHz, C₆D₆): $\delta = 20.6$; ¹³C{¹H} NMR (101 MHz, C₆D₆): $\delta = 24.0$ (CH(CH₃)₂), 24.4 (CH(CH₃)₂), 28.6 (CH(CH₃)₂), 116.0 (NCH), 123.5 (Dipp-*m*-CH), 127.4 (Dipp-*p*-CH), 137.8 (Dipp-*i*-C), 146.8 (Dipp-*o*-C). Compound **5**: analytically calculated for C₂₄H₂₀Be: C, 90.81; H, 6.35. Found: C, 90.48; H, 6.32. ¹H NMR (400 MHz, C₆D₆, 298 K): $\delta = 5.61$ (s, 5H, C₅H₅), 7.03 (t, ³J_{HH} = 7.1 Hz, 6H, *o*-C₆H₅), 7.10 (t, ³J_{HH} = 7.3 Hz, 6H, *m*-C₆H₅), 7.36 (d, ³J_{HH} = 7.6 Hz, 3H, *p*-C₆H₅); ⁹Be NMR (42 MHz, C₆D₆): $\delta = -18.0$ ($w_{1/2} = 29.4$ Hz); ¹³C{¹H} NMR (101 MHz, C₆D₆): 102.7 (C₅H₅), 131.0 (C₆H₅), 137.9 (C₆H₅), 141.5 (C₆H₅), 145.0 (C₆H₅), 187.3 (CPh₃).

Crystallographic data

Crystallographic data for **2–5** were collected using an Oxford Diffraction (Agilent) SuperNova or Rigaku XtaLAB Synergy-R. Crystals were selected under Paratone-N or perfluorinated oil, mounted on MiTeGen Micromount loops and quench-cooled using an Oxford Cryosystems open flow N₂ cooling device⁶⁶. Selected details of data collection are given in Supplementary Table 1. Data collected were processed using the CrysAlisPro package, including unit cell parameter refinement and inter-frame scaling (which was carried out using SCALE3 ABSPACK within CrysAlisPro)⁶⁷. Equivalent reflections were merged and diffraction patterns processed with the CrysAlisPro suite. Structures were solved ab initio from the integrated intensities using SHELXT and refined on F₂ using SHELXL with the graphical interface OLEX2^{68–70}. In the case of complex **3**, the NoSpherA2 method was used for refinement using non-spherical form factors^{59,71}. In this case, r²SCAN def2-SVP was used in the iterative improvement of the fit of the model (followed by a single-point calculation; r²SCAN def2-TZVP) using ORCA version 5.0.4 (refs. 72–76). Crystallographic data are given in the supplementary deposited CIF files (CCDC 2324714–2324717) and can be obtained free of charge from the Cambridge Crystallographic Data Centre via http://www.ccdc.cam.ac.uk/data_request/cif. Structures of **3** and **5** feature disorder of the cyclopentadienyl groups over special positions. This was treated using part –1 and fractional occupancy in both cases. Further details of how crystallographic disorder was treated can be found in the CIF files.

Computational details

The structures of complexes **1–3**, **3'** (compound **3** without potassium cation [(HCDippN)₂BO]₂BeBeCp⁺) and **B–D** were optimized using ORCA (revision 5.0.4)^{72,73}. Specifically, r²SCAN was used^{74,77}, in conjunction with the def2-TZVPPm basis set with the D4 dispersion correction⁷⁸, using the geometrical counterpoise correction gCP (together known as the r²SCAN-3c method) and CPCM solvent (benzene) modelling^{79,80}. Subsequently, a single-point calculation was performed on this optimized structure with the ω B97X range-separated hybrid

functional^{75,81}, in conjunction with the def2-QZVPP basis set^{76,82} and the D4 dispersion correction⁷⁸. The nature of the stationary points (minima) was confirmed by full frequency calculations, which are characterized by zero imaginary frequencies. NBO calculation was performed on the ORCA wavefunction using NBO 7.0 (ref. 83). QTAIM calculations were performed using the ORCA wavefunctions for the respective complexes and were generated using Multiwfn 3.8 and AIMALL^{84,85}. ELF calculations were performed using the ORCA wavefunctions for the respective complexes, generated using Multiwfn 3.8 (ref. 86). All EDA was performed using Gaussian 16 (revision C.01) at the M062x-def2-TZVP level⁸⁷.

Data availability

All data generated or analysed during this study are included in this published article (and its Supplementary Information files). X-ray data are available free of charge from the Cambridge Crystallographic Data Centre (CCDC 2324714 (5), 2324715 (3), 2324716 (2) and 2324717 (4)). Cartesian coordinates of optimized structures are available as a Supplementary Information file.

References

- Bahr, S. R. & Boudjouk, P. Trityl tetrakis[3,5-bis(trifluoromethyl)phenyl]borate: a new hydride abstraction reagent. *J. Org. Chem.* **57**, 5545–5547 (1992).
- Cosier, J. & Glazer, A. M. A nitrogen-gas-stream cryostat for general X-ray diffraction studies. *J. Appl. Crystallogr.* **19**, 105–107 (1986).
- CrysAlisPro (Agilent Technologies, 2013).
- Sheldrick, G. M. Crystal structure refinement with SHELXL. *Acta Crystallogr. C* **71**, 3–8 (2015).
- Sheldrick, G. M. SHELXT—integrated space-group and crystal-structure determination. *Acta Crystallogr. A* **71**, 3–8 (2015).
- Dolomanov, O. V., Bourhis, L. J., Gildea, R. J., Howard, J. A. K. & Puschmann, H. OLEX2: a complete structure solution, refinement and analysis program. *J. Appl. Crystallogr.* **42**, 339–341 (2009).
- Midgley, L. et al. Vanishing of the atomic form factor derivatives in non-spherical structural refinement—a key approximation scrutinized in the case of Hirshfeld atom refinement. *Acta Crystallogr. A* **77**, 519–533 (2021).
- Neese, F. The ORCA program system. *WIREs Comput. Mol. Sci.* **2**, 73–78 (2012).
- Neese, F. Software update: the ORCA program system, version 4.0. *WIREs Comput. Mol. Sci.* **8**, e1327 (2018).
- Grimme, S., Hansen, A., Ehlert, S. & Mewes, J.-M. r²SCAN-3c: a “Swiss army knife” composite electronic-structure method. *J. Chem. Phys.* **154**, (2021).
- Mardirossian, N. & Head-Gordon, M. ωB97X-V: a 10-parameter, range-separated hybrid, generalized gradient approximation density functional with nonlocal correlation, designed by a survival-of-the-fittest strategy. *Phys. Chem. Chem. Phys.* **16**, 9904 (2014).
- Weigend, F. & Ahlrichs, R. Balanced basis sets of split valence, triple zeta valence and quadruple zeta valence quality for H to Rn: design and assessment of accuracy. *Phys. Chem. Chem. Phys.* **7**, 3297 (2005).
- Furness, J. W., Kaplan, A. D., Ning, J., Perdew, J. P. & Sun, J. Accurate and numerically efficient r²SCAN meta-generalized gradient approximation. *J. Phys. Chem. Lett.* **11**, 8208–8215 (2020).
- Caldeweyher, E., Mewes, J.-M., Ehlert, S. & Grimme, S. Extension and evaluation of the D4 London-dispersion model for periodic systems. *Phys. Chem. Chem. Phys.* **22**, 8499–8512 (2020).
- Kruse, H. & Grimme, S. A geometrical correction for the inter- and intra-molecular basis set superposition error in Hartree-Fock and density functional theory calculations for large systems. *J. Chem. Phys.* **136**, 154101 (2012).
- Barone, V. & Cossi, M. Quantum calculation of molecular energies and energy gradients in solution by a conductor solvent model. *J. Phys. Chem. A* **102**, 1995–2001 (1998).
- Najibi, A. & Goerigk, L. DFT-D4 counterparts of leading meta-generalized-gradient approximation and hybrid density functionals for energetics and geometries. *J. Comput. Chem.* **41**, 2562–2572 (2020).
- Weigend, F. Accurate Coulomb-fitting basis sets for H to Rn. *Phys. Chem. Chem. Phys.* **8**, 1057 (2006).
- Glendening, E. D. et al. NBO 7.0 (Theoretical Chemistry Institute, Univ. of Wisconsin, Madison, 2018).
- Todd, K. A. AIMAll (version 19.10.12) (TK Gristmill Software, 2019).
- Lu, T. & Chen, F. Multiwfn: a multifunctional wavefunction analyzer. *J. Comput. Chem.* **33**, 580–592 (2012).
- Silvi, B. & Savin, A. Classification of chemical bonds based on topological analysis of electron localization functions. *Nature* **371**, 683–686 (1994).
- Frisch, M. J. et al. Gaussian 16 (Gaussian, Inc., 2016).

Acknowledgements

J.T.B. thanks St John’s College, Oxford, for a Junior Research Fellowship. We thank the John Fell Fund (0011792) and the Royal Society of Chemistry (Research Fund R23-3176939355) for financial support. We thank the EPSRC Centre for Doctoral Training in Inorganic Chemistry for Future Manufacturing (OxICFM, EP/S023828/1 studentships for A.E.C. and A.F.R.).

Author contributions

J.T.B.: conceptualization, investigation (synthetic and computational), visualization, analysis, writing (original draft), writing (review and editing), funding acquisition, supervision and project administration. A.E.C.: investigation (computational and crystallographic), visualization and writing (review and editing). A.F.R.: investigation (crystallographic) and writing (review and editing). S.A.: funding acquisition, project administration, supervision and writing (review and editing).

Competing interests

The authors declare no competing interests.

Additional information

Supplementary information The online version contains supplementary material available at <https://doi.org/10.1038/s41557-024-01534-9>.

Correspondence and requests for materials should be addressed to Josef T. Boronski or Simon Aldridge.

Peer review information *Nature Chemistry* thanks the anonymous reviewers for their contribution to the peer review of this work.

Reprints and permissions information is available at www.nature.com/reprints.